Modeling Crossflow-Induced Propeller Autorotation

Ryan King
AE451: Aircraft Design II
Clarkson University, Potsdam, NY, USA 13699
May 2nd, 2025

***Abstract*—The design of VTOL aircraft, particularly eVTOL aircraft, often relies on the use of multiple electrically powered thrust-vectoring propellers to meet the high thrust requirements of vertical flight. Many configurations employ aft-mounted propellers fixed in a vertical orientation, dedicated exclusively to providing extra lift during vertical take-off and landing. These propellers, left unpowered at cruise, experience crossflow—air moving parallel to the plane of rotation—which in turn induces autorotation. Modeling the aerodynamic behavior resulting from this crossflow-induced autorotation requires a modified mathematical framework—an adaptation of blade element theory—formulated specifically for crossflow conditions. This report presents the formulation of such a model and introduces software developed to solve it numerically, which, given propeller geometry and initial crossflow conditions, computes both transient and steady-state solutions for the propeller's kinematic and aerodynamic states. These solutions inform the design and optimization of propeller systems for VTOL and eVTOL aircraft by providing insight into design parameters that drive both desired and undesired aerodynamic behavior. Notably, they reveal a strong positive correlation between blade pitch and cruise drag, suggesting that variable-pitch propellers, by leveling the blades at cruise, may offer advantages in improving aerodynamic efficiency.**

Nomenclature

c ..... Blade chord length (m)
C_d ..... Section drag coefficient
C_ℓ ..... Section lift coefficient
D ..... Total propeller drag (N)
D_h ..... Propeller hub drag (N)
D_n ..... Drag from the n^{th} propeller blade (N)
$F_{y,n}$ ..... Side-force from the n^{th} propeller blade (N)
F_y ..... Total propeller side-force (N)
h ..... Propeller hub height (m)
I_z ..... Moment of inertia about the z-axis (kg·m^2)
K_V ..... Motor velocity constant ((rads/s)/V)
K_t ..... Motor torque constant (Nm/A)
L ..... Total propeller lift (N)
L_n ..... Lift from the n^{th} propeller blade (N)
N ..... Number of blades
R ..... Motor winding resistance (Ω)
r ..... Radius (m)
Re_h ..... Hub Reynolds number
R_p ..... Propeller radius (m)
R_h ..... Propeller hub radius (m)
t ..... Time (s)
v_∞ ..... Freestream kinematic viscosity(m^2/s)
$\vec{V}$ ..... Relative velocity vector (m/s)
V_ℓ ..... Relative longitudinal velocity (m/s)
V_t ..... Relative transverse velocity (m/s)
$\vec{V}_\infty$ ..... Freestream velocity vector (m/s)
$\vec{\alpha}$ ..... Angular acceleration vector (rads/s^2)
β ..... Section blade pitch (rads)
θ ..... Propeller angular position (rads)
ρ_∞ ..... Freestream air density (kg/m^3)
τ ..... Net torque (Nm)
τ_a ..... Total Aerodynamic Torque (Nm)
$\tau_{a,n}$ ..... Aerodynamic Torque on the n^{th} blade (Nm)
τ_m ..... Motor torque (Nm)
$\vec{\omega}$ ..... Angular velocity vector (rads/s)

Abbreviations

CFD ..... Computational fluid dynamics
eVTOL ..... Electric vertical take-off and landing
GUI ..... Graphical user interface
SIMD ..... Single instruction, multiple data
VTOL ..... Vertical take-off and landing

I. INTRODUCTION

An unpowered propeller, oriented so that its plane of rotation is parallel to a freestream, will autorotate as energy from the flow is imparted to the propeller's blades. Understanding the aerodynamics of this crossflow-induced autorotation is critical for the design of modern eVTOL aircraft, which often combine the use of forward wing-mounted thrust-vectoring propellers and aft wing-mounted vertically fixed propellers, both of which may experience crossflow-induced autorotation. Modeling this phenomenon requires a novel mathematical approach, as classical blade element theory assumes airflow collinear with the rotation axis, not perpendicular, as in the case of crossflow-induced

autorotation [1]. Adapting classical blade element theory to account for propeller crossflow produces a system of nonlinear ordinary differential equations governing the propeller's motion and aerodynamics. Specialized software developed to numerically solve this system enables detailed analysis of the geometric factors driving transient aerodynamic behavior. This analysis streamlines the optimization of propeller designs for the cruise crossflow conditions.

II. FORMULATION OF A MATHEMATICAL MODEL

To formulate a mathematical model for crossflow-induced autorotation, several simplifying assumptions are introduced. The flow is assumed incompressible, the upstream velocity profile is taken to be linear, and the induced velocity from the propeller's rotation is considered negligible. A coordinate system is established to define the aerodynamic forces acting on the propeller—a foundation for deriving the equations of motion. The following sections detail the governing assumptions, coordinate system, aerodynamic force modeling, and equations of motion for the autorotation.

A. Governing Assumptions

As typically cruising speeds of current eVTOL aircraft fall bellow Mach 0.3, incompressible flow may be assumed if the propeller's maximum tip speed also meets this threshold. Conveniently, angular velocities during autorotation are significantly less than powered operation, producing tip speeds under the Mach 0.3 threshold for reasonably sized propellers. This assumption permits the use of subsonic aerodynamic equations and airfoil experimental data to develop a model for aerodynamic forces.

In addition, the velocity profile is assumed to be linear—an assumption that holds well for propellers mounted ahead of flow-disrupting elements. Whereas when mounted, for example, behind a wing and subject to propeller-shed vortices, the more relevant case, this assumption becomes a likely source of error. Nevertheless, this assumption serves as a clear starting point for a simplified mathematical approach.

Lastly, we assume that velocity induced by the propeller's rotation is negligible. As in the assumption of incompressible flow, the propeller's significantly lower rotation rate during autorotation justifies the simplification. It follows that the formulation avoids the mathematical complications of adapting blade element momentum theory as there is no longer a need to model the propeller's suction produced by a high rotation rate. As such, the mathematical formulation reduces to an adaptation of only bade element theory [2].

B. Coordinate System

The coordinate system for the model's mathematical formulation is shown in Fig. 1.

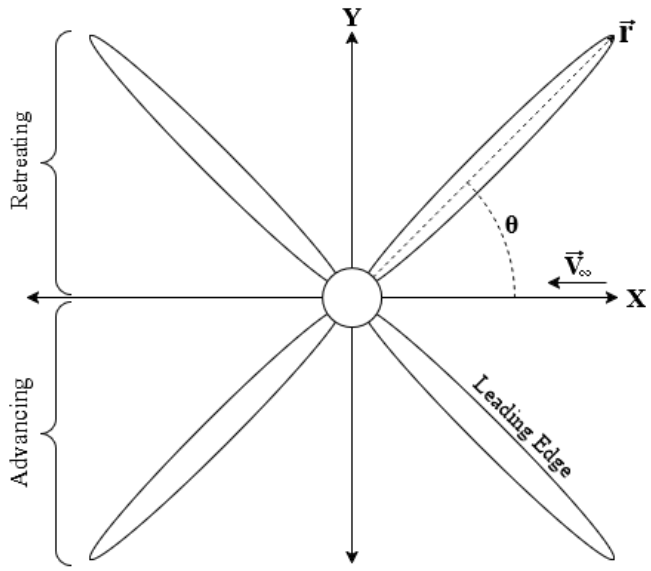

Fig. 1: The right-handed coordinate system for the propeller autorotation model.

The propeller rotates about the z-axis, while the freestream (crossflow) velocity vector, $\vec{V}_\infty$, is directed along the negative x-axis. As the propeller rotates, the blades cyclically pass through regions where they either advance or retreat into the freestream, providing an increase or decrease in the relative velocity, V, as defined in (1).

$$\vec{V} = (\vec{\omega} \times \vec{r}) + \vec{V}_\infty \tag{1}$$

Equation (1) defines the relative velocity as the vector sum of the circular velocity—the cross product of the angular velocity, $\vec{\omega}$, and the radial position vector, $\vec{r}$—and the freestream velocity vector, $\vec{V}_\infty$. This relative velocity is then resolved into two components: one parallel to the blade chord line and one perpendicular to it. The parallel component, referred to as the relative transverse velocity, V_t, is used to compute the aerodynamic forces acting on the blades through integration from the blade root to the blade tip and is given by (2).

$$V_t = \frac{\vec{V} \cdot (\vec{\omega} \times \vec{r})}{\|\vec{\omega} \times \vec{r}\|} \tag{2}$$

The perpendicular component, the relative longitudinal

velocity, is obtained by (3), although it is not used in the subsequent mathematical formulation.

$$V_\ell = \vec{V} \cdot \hat{r} \tag{3}$$

However, incorporating the longitudinal velocity into the aerodynamic force modeling could improve the model's accuracy by capturing drag due to spanwise flow along the blade and should be considered in future work.

C. Modeling Aerodynamic Forces

As in blade element theory, the total aerodynamic forces acting on each blade is estimated by integrating from the blade root at $r = R_h$ to the blade tip at $r = R_p$. Each discretization along the blade's span is taken as an airfoil section of width dr, chord length c, lift coefficient C_ℓ, drag coefficient C_d, and pitch β—all of which are functions of the radial position r. The lift produced by the nth blade is obtained using (4).

$$L_n = \int_{R_h}^{R_p} C_\ell \left(\tfrac{1}{2}\rho_\infty V_t^2\right) c \, dr \tag{4}$$

Similarly, the contribution of aerodynamic torque from the nth blade is found using (5). The sign function is applied to the transverse velocity because the dot product in (2), permits the possibility of reversed airflow (i.e., from the blade's nominal trailing edge to the blade's nominal leading edge) when a retreating blade moves faster than the opposing freestream. In such cases, aerodynamic torque is clockwise.

$$\tau_{a,n} = \int_{R_h}^{R_p} C_d \left(\tfrac{1}{2}\rho_\infty V_t^2\right) cr \, \mathrm{sgn}(V_t) \, dr \tag{5}$$

To compute the propeller drag contribution from each blade, the sine of the angular position, θ, is introduced in the integration to extract the x-axis component of the airfoil section drag, as shown in (6).

$$D_n = \int_{R_h}^{R_p} C_d \left(\tfrac{1}{2}\rho_\infty V_t^2\right) c \, \mathrm{sgn}(V_t) \sin\theta \, dr \tag{6}$$

By instead using the cosine function, the side-force, F_y, acting along the y-axis, may be obtained from (7).

$$F_{x,n} = \int_{R_h}^{R_p} C_d \left(\tfrac{1}{2}\rho_\infty V_t^2\right) c \, \mathrm{sgn}(V_t) \cos\theta \, dr \tag{7}$$

Notably, the lift and drag coefficients used in (4)-(7) are functions of the section angle of attack, section Reynolds number, and direction of flow—either nominal or reversed. Additionally, the blade pitch, β, is the geometric angle of attack for each section, since, unlike classical blade element theory, there is no freestream velocity component parallel to the rotation axis [1]. Numerical solution of the model requires experimental data for the propeller's airfoil(s) across a range of angles of attack and Reynolds numbers.

The total lift, drag, torque, and side-force for the propeller is obtained by summing the relevant contributions from each blade; however, the hub drag and the motor's resistive torque are also included in the summations. The hub drag is determined by first calculating the hub Reynolds number given by (8).

$$Re_h = \frac{2R_h\|\vec{V}_\infty\|}{v_\infty} \tag{8}$$

Using the hub Reynolds number, the hub drag is estimated from the piecewise function, (9), which is derived from experimental data reported by Brennen [3].

$$D_h = \begin{cases} \left({}^{24}/_{Re_h}\right)\left(\frac{1}{2}\rho_\infty\|\vec{V}_\infty\|^2\right)h & Re_h < 10 \\ \left(2.42 - \frac{Re_h}{2000}\right)\left(\frac{1}{2}\rho_\infty\|\vec{V}_\infty\|^2\right)h & 10 \le Re_h < 10^3 \\ \left({}^{1}/_{2}\right)\left(\frac{1}{2}\rho_\infty\|\vec{V}_\infty\|^2\right)h & 10^3 \le Re_h < 3\text{e}5 \\ \left({}^{3}/_{20}\right)\left(\frac{1}{2}\rho_\infty\|\vec{V}_\infty\|^2\right)h & Re_h \ge 3\text{e}5 \end{cases} \tag{9}$$

Secondly, the electric motor's resistive torque, τ_m, is obtained using (10), which models the motor's internal resistance to rotation using the motor velocity constant, K_v, torque constant, K_t, and motor winding resistance, R.

$$\tau_m = \frac{K_t\omega}{K_v R} \tag{10}$$

Incorporating (9) and (10), the total lift, drag, side-force, and net torque are calculated using (11)–(14), respectively.

$$L = \sum_{n=1}^{n=N} L_n \tag{11}$$

$$D = \left(\sum_{n=1}^{n=N} D_n\right) + D_h \tag{12}$$

$$F_y = \sum_{n=1}^{n=N} F_{y,n} \tag{13}$$

$$\tau = \left(\sum_{n=1}^{n=N} \tau_{a,n}\right) - \tau_m \tag{14}$$

D. Equations of Motion

As computing the total aerodynamic forces requires the instantaneous angular position and velocity, a system of equations is developed to model the propeller's kinematic state over time. Using the system's moment of inertia about the z-axis, (15) relates the instantaneous torque, $\tau(t)$, to the instantaneous angular acceleration, $\alpha(t)$.

$$\alpha(t) = \frac{\tau(t)}{I_z} \tag{15}$$

The time derivatives of angular velocity and angular position are derived from standard rigid body dynamics and expressed in (16) and (17), respectively.

$$\frac{d\omega}{dt} = \alpha(t) \quad (16)$$

$$\frac{d\theta}{dt} = \omega(t) \quad (17)$$

The two equations form a system of nonlinear ordinary differential equations that can be solved numerically using a fourth-order Runge-Kutta scheme.

III. SOLVING THE MODEL NUMERICALLY

To apply the Runge-Kutta scheme to the equations of motion, the aerodynamic coefficients for the propeller's airfoil(s) must be determined over a range of angles of attack and Reynolds numbers for both nominal and reversed flow conditions. Furthermore, custom software is developed that implements the fourth-order Runge-Kutta algorithm to solve the equations of motion given propeller geometry and crossflow conditions. For the purposes of this paper, the AE451 Mission III eVTOL aircraft's aft propeller design is used as a case study. The propeller's general configuration is provided in Table I, and the blade geometry is listed in Table II.

TABLE I. PROPELLER CONFIGURATION

Propeller Radius (R_p)	1.5 m
Hub Radius (R_h)	0.18 m
Hub Height (h)	0.2 m
Number of Blades (N)	4
Blade Airfoil	DAE-51

TABLE II. PROPELLER BLADE GEOMETRY

Radius (% Span)	Blade Chord (m)	Blade Pitch (deg)
0 (r=R_h)	0.0667	55.9
10	0.1333	55.9
20	0.2205	55.9
30	0.2499	48.9
40	0.2646	42.3
50	0.2499	37.2
60	0.2352	32.8
70	0.2205	30.0
80	0.1764	26.4
90	0.1370	24.3
100 (r=R_p)	0.0000	22.5

A. *Using ANSYS Fluent for Airfoil CFD*

ANSYS Fluent is used to perform computational fluid dynamics (CFD) on the DAE-51 airfoil under both nominal and reversed flow conditions at a Reynolds number of 10^6. During numerical integration, the software interpolates aerodynamic data between blade pitch and Reynolds numbers at each radial discretization. The resulting lift and drag coefficients—between angles of attack from −20° to 55° for both nominal and reversed flows—are presented in Fig. 2.

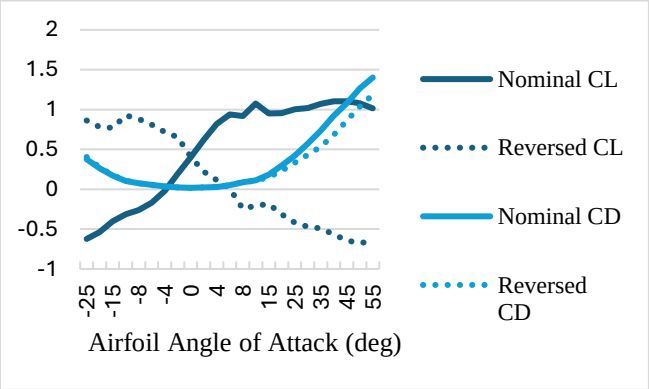

Figure 2: Nominal and reversed aerodynamic coefficients of a DAE-51 airfoil at a Reynolds number of 10^6.

Results from the airfoil analyses demonstrate expected aerodynamic behavior between -15° and 15°, encompassing the primary interpolation range of the model. However, the ANSYS Fluent simulations do not capture the anticipated flow separation at higher angles of attack, which typically results in a decrease in the lift coefficient. Improving the ANSYS Fluent model by incorporating turbulence modeling techniques could better capture this phenomenon, reducing error—a necessary focus for future work.

The reversed flow condition is not widely studied, so a velocity magnitude contour for an E193 airfoil at a 5° angle of attack is also provided in Fig. 3 for reference.

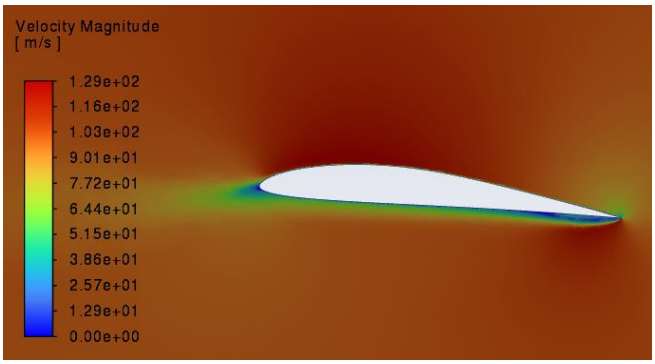

Figure 3: ANSYS Fluent velocity magnitude contour of an E193 airfoil at a 5° angle of attack during reversed flow (right to left).

B. *Developing Specialized Software*

Owing to the nonlinearity of the equations of motion, the system of differential equations must be solved numerically. Initial implementations used MATLAB; however, due to MATLAB's computational inefficiency, a lower-level, high-performance solver was required. Consequently, replacement software was developed in C++, enabling the same calculations to be executed in a fraction of the time. By leveraging C++ compile-time evaluation and SIMD

intrinsics, computational time was reduced by more than 99%—from several minutes to under a second. Additionally, a graphical user interface (GUI) was implemented to facilitate real-time adjustments of multiple sets of parameters. The source code and software is publicly available on GitHub [4].

C. *Numerical Solution Procedure and RK4 Implementation*

To perform the RK4 integration, the solver propagates the propeller's kinematic and aerodynamic states over discrete time steps. At each time step, the net torque is calculated using (14) and substituted into (15) to obtain the angular acceleration. The angular acceleration is used to update angular velocity and angular position via. the RK4 method. Simultaneously, lift, drag, side-force, and motor torque are calculated based on the updated state. Aerodynamic forces along the blade radius are evaluated by interpolating from a precomputed matrix of airfoil characteristic curves at various Reynolds numbers (see Fig. 2). The result is a solution of all the system's state variables over the full simulation time. Notably, as the system is an initial value problem, an initial angular position, velocity, and acceleration must be provided to initiate numerical integration.

IV. VALIDATION

Software validation is conducted by comparing static lift calculations from the C++ software with those obtained from PropCalc, a blade-element momentum model. The results are shown for a range of tested RPMs.

TABLE III. SOFTWARE VALIDATION

Test Case	C ++ Model	PropCalc	Error
1000 RPM	41 N	45 N	8.89 %
2050 RPM	215 N	195 N	10.3 %
3550 RPM	512 N	590 N	13.2 %
4550 RPM	842 N	990 N	14.9 %
5550 RPM	1253 N	1450 N	16.5 %

As the error remained relatively low throughout the validation tests, with only slight increases as compressibility effects became more dominant, one can be confident in the model's ability to accurately predict lift and similarly calculated aerodynamic parameters. However, as this is the only validation procedure, future work should emphasize the validation of the transient solutions for all state variables.

V. RESULTS

The propeller test geometry and the aircraft parameters in Table IV are substituted into the developed software to compute both the transient and steady-state solutions for the propeller's angular velocity, lift, drag, torque, and side-force. Secondly, the blade's pitch is decreased by a constant 38.25° along the span and a second analysis is performed to investigate the aerodynamics of a variable-pitch propeller.

TABLE IV. AIRCRAFT PARAMETERS

Freestream Velocity ($\|\vec{V}_\infty\|$)	87 m/s
Air Density (ρ_∞)	1.167 kg/m^3
Kinematic Viscosity (v_∞)	1.520e-5 m^2/s
Motor Velocity Constant (K_v)	1.750 (rads/s)/V
Motor Winding Resistance (R)	0.125 Ω
Motor Torque Constant (K_t)	0.0909 Nm/A
Moment of Inertia (I_z)	10 kg·m^2

A. *Results for the Test Case Propeller*

Starting from rest, the system attains a steady state within one second, at which point the net torque oscillates about zero, causing small perturbations in the angular velocity. Fig. 4 shows the transient response of the propeller's angular velocity, settling at an average of 45 RPM.

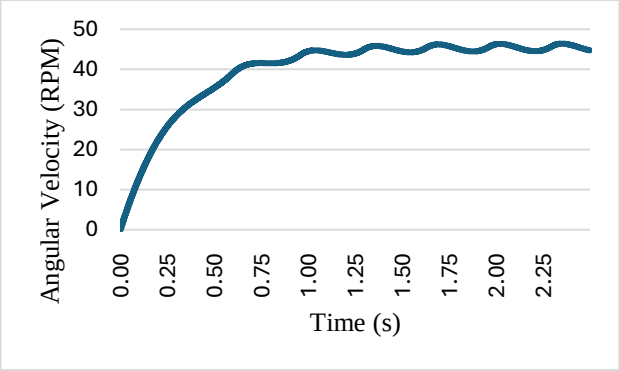

Figure 4: Temporal solution for angular velocity.

These small perturbations in the angular velocity—coupled with cyclic changes in the angular position—yield an even larger oscillatory response for lift and drag, as shown in Fig. 5.

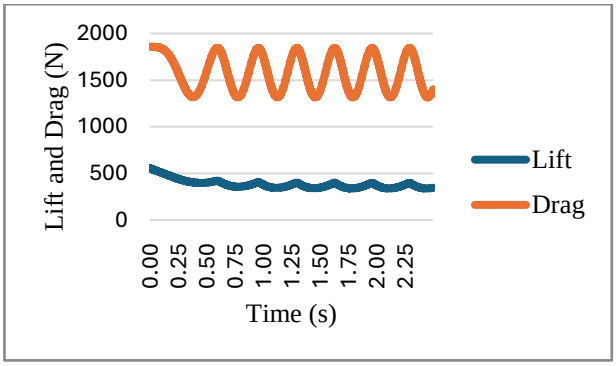

Figure 5: Temporal solution for lift and drag.

Here, drag peaks at 1.85 kN per propeller; with four aft propellers, this consumes more than the aircraft's entire 4.06 kN drag budget. Clearly geometric modifications must be made to improve the propeller's aerodynamic design. The remaining solutions, side-force and torque are shown in Fig. 6 and Fig. 7, respectively. Each solution exhibits oscillatory behavior as the blades sweep through different angular positions.

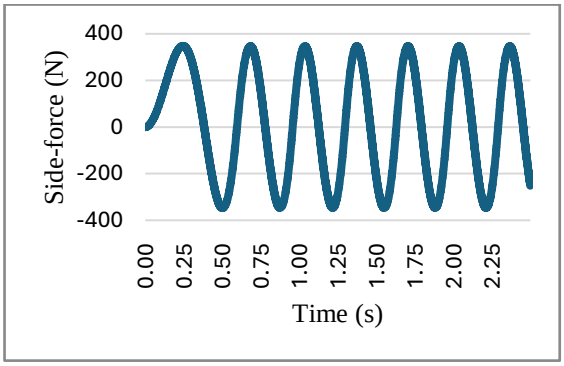

Figure 6: Temporal solution for side-force.

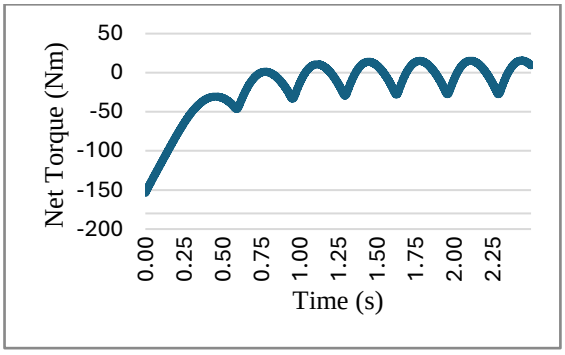

Figure 7: Temporal solution for net torque.

B. Results for the Variable-pitch Propeller

To improve the propeller's aerodynamic efficiency, the blade pitch is reduced by 38.25° along the span to simulate the effect of using a variable-pitch propeller to level the blades during cruise. The resulting lift and drag solutions are shown in Fig. 8.

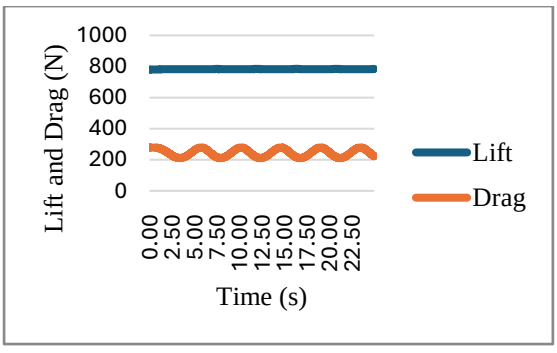

Figure 8: Leveled propeller temporal solution for lift and drag.

As demonstrated, the use of a variable-pitch propeller can substantially reduce drag during crossflow-induced autorotation. By leveling the test propeller's blades, peak drag per propeller decreased from 1.85kN to 0.28 kN. Furthermore, the total drag from the aircraft's four aft propellers will now total 980 N, only 24% of the aircraft's drag budget—an 84% reduction from the fixed-pitch propeller configuration.

VI. CONCLUSION

In this work, blade element theory is adapted to formulate a mathematical model for crossflow-induced autorotation. The model is then solved numerically using a fourth-order Runge-Kutta implementation in custom C++ software. Applying this model to the AE451 Mission III eVTOL aircraft's propeller revealed that utilizing variable-pitch propeller configurations can significantly reduce aerodynamic drag during cruise, achieving an 84% decrease compared to the fixed-pitch propeller configuration. Future enhancements to the model could include incorporating relative longitudinal velocity in aerodynamic force calculations, refining the ANSYS Fluent airfoil model, conducting computational fluid dynamics (CFD) analyses across a broader range of Reynolds numbers, and performing further validation to improve accuracy.

VII. REFERENCES

[1] H. Glauert, "The Airscrew: Blade Element Theory," in *The Elements of Aerofoil and Airscrew Theory*, London: Cambridge University Press, 1926, pp. 208–222

[2] H. Glauert, "The Airscrew: Momentum Theory," in *The Elements of Aerofoil and Airscrew Theory*, London: Cambridge University Press, 1926, pp. 199–208

[3] C. E. Brennen, "An Internet Book on Fluid Dynamics: Drag on a Sphere and Cylinder". Pasadena, CA: California Institute of Technology, 2006. [Online]. Available: http://brennen.caltech.edu/fluidbook/externalflows/drag/dragonasphere.pdf

[4] R. King, "Propeller Crossflow Autorotation Solver (v1.0.0)," Apr. 2025. [Source code]. Available:https://github.com/RyanKingSoftware/propeller-crossflow-autorotation-solver